Princeton Plasma Physics Laboratory

PPPL- 4436

PPPL- 4436

Shielding of External Magnetic Perturbations By Torque In Rotating Tokamak Plasmas

Jong-Kyu Park, Allen H. Boozer, Jonathan E. Menard,
Stefan P. Gerhardt, and Steve A. Sabbagh

August, 2009

PPPL
PRINCETON PLASMA
PHYSICS LABORATORY

Prepared for the U.S. Department of Energy under Contract DE-AC02-09CH11466.

Princeton Plasma Physics Laboratory
Report Disclaimers

Full Legal Disclaimer

Trademark Disclaimer

PPPL Report Availability

Princeton Plasma Physics Laboratory:

http://www.pppl.gov/techreports.cfm

Office of Scientific and Technical Information (OSTI):

http://www.osti.gov/bridge

Related Links:

U.S. Department of Energy

Office of Scientific and Technical Information

Fusion Links

Shielding of external magnetic perturbations by torque in rotating tokamak plasmas

Jong-Kyu Park,[1] Allen H. Boozer,[2] Jonathan E. Menard,[1] Stefan P. Gerhardt,[1] and Steve A. Sabbagh[2]

[1]*Princeton Plasma Physics Laboratory, Princeton, New Jersey, NJ 08543*

[2]*Department of Applied Physics and Applied Mathematics, Columbia University, New York, NY 10027*

(Dated: August 21, 2009)

Abstract

The imposition of a nonaxisymmetric magnetic perturbation on a rotating tokamak plasma requires energy and toroidal torque. Fundamental electrodynamics implies that the torque is essentially limited and must be consistent with the external response of a plasma equilibrium $\vec{f} = \vec{j} \times \vec{B}$. Here magnetic measurements on National Spherical Torus eXperiment (NSTX) device are used to derive the energy and the torque, and these empirical evaluations are compared with theoretical calculations based on perturbed scalar pressure equilibria $\vec{f} = \vec{\nabla} p$ coupled with the theory of nonambipolar transport. The measurement and the theory are consistent within acceptable uncertainties, but can be largely inconsistent when the torque is comparable to the energy. This is expected since the currents associated with the torque are ignored in scalar pressure equilibria, but these currents tend to shield the perturbation.

I. INTRODUCTION

Tokamaks, such as International Thermonuclear Energy Reactor (ITER) [1], are sensitive to magnetic perturbations caused by nonaxisymmetric currents external to the plasma. These perturbations can lead to a significant degradation of confinement [2–4], but also can be used to improve the performance [5, 6]. A tokamak plasma responds to a nonaxisymmetric magnetic perturbation by producing perturbed plasma currents. These currents can fundamentally change the magnetic perturbation as shown in the calculations of perturbed scalar pressure equilibria using Ideal Perturbed Equilibrium Code (IPEC) [7], and in the IPEC applications to plasma locking experiments [8, 9].

Magnetic perturbations are both amplified and phase shifted by the plasma response [10], as has been demonstrated in a number of Resonant Field Amplification (RFA) measurements [11–14]. The amplification and the phase shift by small perturbations are related to the perturbed energy and toroidal torque, which thus can be derived from magnetic measurements. These derived energy and torque can be compared with the calculations if any relevant model exists. The study in this paper uses and simplifies the exact relation for the plasma response to evaluate the energy and the torque from magnetic measurements on National Spherical Torus eXpeiment (NSTX) device [15]. The empirically evaluated energy and torque are compared with the theoretical calculations based on perturbed scalar pressure equilibria coupled with the theory of nonambipolar transport [16–19].

This paper shows that magnetic perturbations are shielded in the presence of a torque in comparison to perturbed scalar pressure equilibria, which do not include the torque. The exact relation for the plasma response to the energy and the torque [10] will be discussed to illustrate the fundamental implication of the shielding by the torque (Sec. II). The plasma response can be measured by magnetic sensors, but one needs to include the currents at the wall if the sensors close to the wall are used to derive the energy and the torque from the measurements (Sec. III). The presented method in Sec. III is based on the extensive work in [10, 20], but is different since this paper describes the relation that is directly applicable to RFA measurements. Using the relation in Sec. III, the energy and the torque are empirically derived from NSTX $n = 1$ RFA measurements (Sec. IV), and are compared with the calculations using IPEC coupled with the theory of nonambipolar transport (Sec. V). The comparison between experiment and theory indicates that the shielding by torque

becomes important in high β_N plasmas, and so the tensor pressure must be included in the calculations of perturbed equilibria.

II. EXACT RELATION FOR PLASMA RESPONSE AND IMPLICATION

Any plasma equilibria obeys $\vec{f} = \vec{j} \times \vec{B}$, and the fundamental electrodynamics gives [10]

$$2\delta W + i\frac{\tau_\varphi}{n} = \vec{\Phi}^\dagger \cdot \overleftrightarrow{L}_p^{-1} \cdot \vec{\Phi}^x \tag{1}$$

at the plasma boundary surface with the surface inductance $\overleftrightarrow{L}_p$. Equation (1) provides the exact relation of interaction between the plasma and small external perturbations. The relation implies that the energy δW and the toroidal torque τ_φ determine the amplification and the toroidal phase shift of the plasma response, which is the ratio of the *total flux* $\vec{\Phi}$ to the applied *external flux* $\vec{\Phi}^x$ at the boundary.

The Equation (1) is independent of the model $\vec{f}$. The energy $\delta W = (1/2)\int \delta\vec{j}\cdot\delta\vec{A}d^3x$ and the toroidal torque $\tau_\varphi = -\hat{z}\cdot\int \vec{x}\times(\delta\vec{j}\times\delta\vec{B})d^3x$ are produced by external perturbations, where $\delta\vec{j}$ is the perturbed current, $\delta\vec{A}$ is the perturbed vector potential, $\delta\vec{B}$ is the perturbed field, and $\hat{z}$ is the symmetry axis of the tokamak. By integrating by parts for δW and τ_φ, the perturbed energy and torque can be related to the total normal field at the boundary and the external currents producing the total normal field. The total normal field can be represented by the total flux

$$\Phi_{mn} = \frac{1}{(2\pi)^2}\oint d\vartheta \oint d\varphi \mathcal{J}(\delta\vec{B}\cdot\vec{\nabla}\psi)e^{-i(m\vartheta-n\varphi)}, \tag{2}$$

where $\mathcal{J}$ is the Jacobian of magnetic coordinates (ψ,ϑ,φ). The expansion coefficients in Equation (2) can be taken to be the elements of a matrix vector $\vec{\Phi}$. A matrix vector for the external flux $\vec{\Phi}^x$ can be defined in the same way, but without the plasma response. The external currents driving the flux can be represented by an equivalent surface current $\vec{K} = \vec{\nabla}\kappa(\vartheta,\varphi)\times\vec{\nabla}\psi$. The surface current potential $\kappa(\vartheta,\varphi)$ can be decomposed as

$$\mathcal{I}_{mn} = \frac{1}{(2\pi)^2}\oint d\vartheta \oint d\varphi \kappa(\vartheta,\varphi)e^{-i(m\vartheta-n\varphi)}, \tag{3}$$

and a matrix vector $\vec{\mathcal{I}}$ can be defined with $\mathcal{I}_{mn}$. The external current $\vec{\mathcal{I}}$ supports the perturbed equilibrium, and produces the external flux in vacuum through $\vec{\Phi}^x = \overleftrightarrow{L}_p\cdot\vec{\mathcal{I}}$. Using the representations of the normal field and the external current, one can derive Equation (1) [10, 20].

External magnetic measurements can determine $\vec{\Phi}$ and $\vec{\Phi}^x$, so they can determine δW and τ_φ. If a model for $\vec{f}$ exists, then one can also theoretically calculate δW and τ_φ. While making comparisons between experiment and theory, it is useful to normalize the energy and the torque as

$$s + i\alpha \equiv -\frac{\vec{\Phi}^\dagger \cdot \overleftrightarrow{L}_p^{-1} \cdot \vec{\Phi}^x}{\vec{\Phi}^\dagger \cdot \overleftrightarrow{L}_p^{-1} \cdot \vec{\Phi}}, \tag{4}$$

and so

$$2\delta W + i\frac{\tau_\varphi}{n} = -(s + i\alpha)\vec{\Phi}^\dagger \cdot \overleftrightarrow{L}_p^{-1} \cdot \vec{\Phi}. \tag{5}$$

That is, magnetic measurements in an experiment can determine (s_E, α_E), which would be consistent with theoretical (s_T, α_T) if the equilibrium model of $\vec{f}$ is correct. This is what is studied in this paper, with RFA measurements in NSTX and the calculations of perturbed scalar pressure equilibria $\vec{f} = \vec{\nabla} p$ coupled with the theory of nonambipolar transport.

Note that knowledge of two independent magnetic quantities such as $\vec{\Phi}$ and $\vec{\Phi}^x$ are required to determine both the energy and the torque in experiments. For instance, a torque analysis of the internal plasma instability [21] requires the measurements of two quantities such as the normal and the tangential components of the total field $\delta\vec{B}(\theta, \varphi)$. Also, one can use the two different sensors as illustrated in [20], but our experiments are easier since the applied $\vec{\Phi}^x$ is known and thus only the plasma response $\vec{\Phi}$ needs to be measured using the same set of magnetic sensors.

The derived relations for the plasma response indicate that the torque in the perturbed plasma is essentially limited given an external flux $\vec{\Phi}^x$ [22]. Equations (1) and (5) imply, using the well known Schwartz inequality

$$\frac{(\vec{\Phi}^\dagger \cdot \overleftrightarrow{L}_p^{-1} \cdot \vec{\Phi}^x)(\vec{\Phi}^{x\dagger} \cdot \overleftrightarrow{L}_p^{-1} \cdot \vec{\Phi})}{(\vec{\Phi}^\dagger \cdot \overleftrightarrow{L}_p^{-1} \cdot \vec{\Phi})(\vec{\Phi}^{x\dagger} \cdot \overleftrightarrow{L}_p^{-1} \cdot \vec{\Phi}^x)} \leq 1, \tag{6}$$

that $(\vec{\Phi}^\dagger \cdot \overleftrightarrow{L}_p^{-1} \cdot \vec{\Phi})/(\vec{\Phi}^{x\dagger} \cdot \overleftrightarrow{L}_p^{-1} \cdot \vec{\Phi}^x) \leq 1/(s^2 + \alpha^2)$. Equation (6) gives the limitation of the torque by

$$\left|\frac{\tau_\varphi}{n}\right| \leq \frac{|\alpha|}{s^2 + \alpha^2}\vec{\Phi}^{x\dagger} \cdot \overleftrightarrow{L}_p^{-1} \cdot \vec{\Phi}^x \leq \frac{\vec{\Phi}^{x\dagger} \cdot \overleftrightarrow{L}_p^{-1} \cdot \vec{\Phi}^x}{2|s|}. \tag{7}$$

Equation (7) shows that the maximum possible torque at a given $|s|$ occurs at $|\alpha| = |s|$. When $s^2 + \alpha^2 << 1$, the toroidal phase shift between the applied field $\vec{\Phi}^x$ and $\vec{\Phi}$ is $n\Delta\phi = \arcsin(\alpha/\sqrt{s^2 + \alpha^2})$ and becomes 45° when $|\alpha| = |s|$. When $\alpha = 0$, the plasma can minimize δW, which makes $|s|$ as small as possible, by distorting the equilibrium currents in such a

way that they amplify the perturbation. When the phase shift reaches 45°, the perturbation is so distorted that it is no longer optimally amplified. That is, the torque is expected to cause shielding unless $|\alpha| << |s|$. This shielding reduces the torque, and hence $|\alpha|$, and increases the energy, and hence $|s|$, required to perturb the plasma.

III. RELATION BETWEEN PLASMA RESPONSE AND RFA MEASUREMENT

The empirical values (s_E, α_E) can be determined using Equation (4) if one can directly measure $\vec{\Phi}$ and $\vec{\Phi}^x$ at the plasma boundary. However, the magnetic sensors are not located at the plasma boundary, but instead are close to the chamber walls. That is, measured quantities in practice are much closer to $\vec{\Phi}_w$ and $\vec{\Phi}^x_w$ at the walls, rather than $\vec{\Phi}$ and $\vec{\Phi}^x$ at the plasma boundary. Note that here the wall is an approximate projection of complicated conducting structures that would require the full numerical modeling, as in VALEN3D code [23], to be more precise.

The two measurements at the walls can be related as $\vec{\Phi}_w = \overleftrightarrow{\mathcal{S}} \cdot \vec{\Phi}^x_w$, where $\overleftrightarrow{\mathcal{S}}$ should include the effects of the currents at the wall. The ratio, $\vec{\Phi}_w/\vec{\Phi}^x_w$, is called Resonant Field Amplification (RFA) [10] in this paper, while $(\vec{\Phi}_w/\vec{\Phi}^x_w) - 1$ is used in other articles [11–14]. The relation between $\overleftrightarrow{\mathcal{S}}$ and (s_E, α_E) can be expressed in terms of inductance coefficients and so-called the permeability of the plasma $\overleftrightarrow{P}$. The plasma permeability $\overleftrightarrow{P}$ is defined by noting that in any plasma state the magnetic field normal to the boundary surface $\delta\vec{B} \cdot \hat{n}$ and the externally produced magnetic field normal to the boundary surface $\delta\vec{B}^x \cdot \hat{n}$ can be related as

$$\vec{\Phi} = \overleftrightarrow{P} \cdot \vec{\Phi}^x. \tag{8}$$

Equation (5) implies that the characteristic permeability is given by $P^{-1} \equiv (\vec{\Phi}^\dagger \cdot \overleftrightarrow{L}_p^{-1} \cdot \overleftrightarrow{P}^{-1} \cdot \vec{\Phi}^x)/(\vec{\Phi}^\dagger \cdot \overleftrightarrow{L}_p^{-1} \cdot \vec{\Phi}) = -(s + i\alpha)$.

To derive $\overleftrightarrow{\mathcal{S}}$, note that the flux through the chamber walls $\vec{\Phi}_w$ is proportional to the currents at the walls $\vec{I}_w$, the currents in circuits outside the wall $\vec{I}_o$, and the currents that represent the plasma response $\vec{I}_p$. If we assume the currents outside the walls are just outside,

$$\vec{\Phi}_w = \overleftrightarrow{L}_w \cdot (\vec{I}_w + \vec{I}_o) + \overleftrightarrow{M}_{wp} \cdot \vec{I}_p, \tag{9}$$

where $\overleftrightarrow{L}_w$ is the surface inductance of the wall and $\overleftrightarrow{M}_{wp} = \overleftrightarrow{M}_{pw}$ is the mutual surface inductance between the plasma and the wall. Using the relation for the currents by plasma

response, $\vec{I}_p = \overleftrightarrow{L}_p^{-1} \cdot (\vec{\Phi} - \vec{\Phi}^x)$, with $\vec{\Phi} = \overleftrightarrow{P} \cdot \vec{\Phi}^x$ in Equation (8), and the relation for the external flux on the plasma, $\vec{\Phi}^x = \overleftrightarrow{M}_{pw} \cdot (\vec{I}_w + \vec{I}_o)$, one can rewrite Equation (9) as

$$\vec{\Phi}_w = \overleftrightarrow{\sigma}^{-1} \cdot \overleftrightarrow{L}_w \cdot (\vec{I}_w + \vec{I}_o), \tag{10}$$

where

$$\overleftrightarrow{\sigma} \equiv (\overleftrightarrow{L}_w \cdot \overleftrightarrow{M}_{pw}^{-1}) \cdot \overleftrightarrow{P}^{-1} \cdot \overleftrightarrow{\Pi} \cdot (\overleftrightarrow{L}_w \cdot \overleftrightarrow{M}_{pw}^{-1})^{-1}, \tag{11}$$

$$\overleftrightarrow{\Pi}^{-1} \equiv (\overleftrightarrow{1} - \overleftrightarrow{C}) \cdot \overleftrightarrow{P}^{-1} + \overleftrightarrow{C}, \quad \text{and} \tag{12}$$

$$\overleftrightarrow{C} \equiv \overleftrightarrow{M}_{pw} \cdot \overleftrightarrow{L}_w^{-1} \cdot \overleftrightarrow{M}_{wp} \cdot \overleftrightarrow{L}_p^{-1}. \tag{13}$$

The $\overleftrightarrow{C}$ is a positive matrix and provides the wall-plasma coupling. The plasma is unstable even with a perfectly conducting wall unless all the eigenvalues of $\overleftrightarrow{\Pi}^{-1}$ have positive real parts, and is unstable with a resistive wall, by the Resistive Wall Mode (RWM), unless all the eigenvalues of $\overleftrightarrow{P}^{-1}$ have positive real parts. In the absence of a plasma, $\overleftrightarrow{P} = \overleftrightarrow{\Pi} = \overleftrightarrow{\sigma} = \overleftrightarrow{1}$.

The external flux through the wall due to the currents in circuits outside the wall is $\vec{\Phi}_w^x \equiv \overleftrightarrow{L}_w \cdot \vec{I}_o$, so one can relate the $\vec{\Phi}_w$ and $\vec{\Phi}_w^x$ using Equation (10) if the currents at the walls $\vec{I}_w$ is known. The evolution equation for the flux through the wall is $d\vec{\Phi}_w/dt = -\overleftrightarrow{R}_w \cdot \vec{I}_w$, where the $\overleftrightarrow{R}_w$ is the resistance matrix of the wall. If applied perturbations are rotating, $d\vec{\Phi}_w/dt = in\omega_a\vec{\Phi}_w$ and so $\vec{I}_w = -in\omega_a\overleftrightarrow{R}_w^{-1} \cdot \vec{\Phi}_w$, where $\omega_a = 2\pi f_a$ is an angular frequency. Therefore, again one can rewrite Equation (10) by replacing $\vec{I}_o$ and $\vec{I}_w$, and can obtain

$$\vec{\Phi}_w = \overleftrightarrow{\mathcal{S}} \cdot \vec{\Phi}_w^x, \tag{14}$$

where

$$\overleftrightarrow{\mathcal{S}}^{-1} \equiv \overleftrightarrow{\sigma} + in\omega_a\overleftrightarrow{L}_w \cdot \overleftrightarrow{R}_w^{-1}. \tag{15}$$

This is the generalized relation for RFA, $\vec{\Phi}_w/\vec{\Phi}_w^x$.

The relations in Equations (14) requires the complete knowledge of all the matrices. Instead, here a simplified relation will be used by assuming that only a single dominant mode is perturbed. This is a good approximation unless the applied field greatly deviates from the dominant external field. The midplane coils and sensors in NSTX are located in the outboard section, so they can effectively produce and measure the dominant external field [8, 24]. The dominant external field is the least stable mode in the sense of stability analysis. Since even the second least stable mode has much higher δW than the least stable mode, mostly up to an order of magnitude, other modes except the least stable mode have

much smaller contributions to RFA if the applied field is reasonably close to the least stable mode. This dominance of the least stable mode may become weaker if a plasma has very low or very high pressure, but this is not the case for plasmas studied in this paper.

In the approximation with a single dominant mode, $\overleftrightarrow{C} \approx c$, $\overleftrightarrow{L}_w \cdot \overleftrightarrow{R}_w^{-1} \approx \gamma_w^{-1}$ and Equation (14) becomes

$$\frac{\Phi_w}{\Phi_w^x} = -\left(\frac{s+i\alpha}{c-(1-c)(s+i\alpha)} - \frac{in\omega_a}{\gamma_w}\right)^{-1}. \tag{16}$$

This equation can be used to determine (s, α) through RFA measurements. The determination of (s_E, α_E) using this equation is essentially identical to the determination of the complex growth rates for RMW [14], which is a function of (s, α).

IV. RFA MEASUREMENT IN NSTX AND EMPIRICAL DERIVATION

The measurements of plasma response $\vec{\Phi}_w$, called RFA measurements, have been performed assuming a single dominant mode for a toroidal harmonic n, since the number of magnetic sensors are not sufficient to determine the detailed shape of the plasma response. That is, Equation (16) is directly applied to the typical RFA measurements of Φ_w/Φ_w^x. In the previous RFA measurements, it has been found that a dominant parameter is the normalized plasma pressure, $\beta_N \equiv 40\pi(aB/\mu_0 I)\langle 2\mu_0 p/B^2\rangle$, where the a is the minor radius, and the I is the toroidal plasma current. This is consistent with the expectation from an ideal MagnetoHydrodynamic (MHD) theory since β_N is the dominant parameter to determine δW, or equivalently s. So, our experiments in NSTX also measured the plasma response as a function of β_N, $(\Phi_w/\Phi_w^x)(\beta_N)$.

The determination of four parameters, $s(\beta_N)$, $\alpha(\beta_N)$, $c(\beta_N)$, and $\gamma_w(\beta_N)$ requires more information than the amplification and the toroidal phase shift at each β_N. In principle, such information with two different frequencies can provide the same number of equations as the number of unknowns at each β_N, but even it does not guarantee the complete determination of the four parameters due to the nonlinear feature of Equation (16). Also, it is difficult to interpret the absolute value of the toroidal phase shift between Φ_w and Φ_w^x due to their different $\phi = 0$ locations, which may be also sensitive to the poloidal location of magnetic sensors. Since the amplitude of RFA is the more reliable information than the phase of RFA, our experiments used the two different frequencies $f_a = \pm 30 Hz$ for a rotating magnetic field in order to make the amplitude of RFA stronger. This is based on the previous observations

in NSTX, which have indicated that the peak of RFA can be found in the co-rotating field with the range of frequency $f_a = +30 \sim +60Hz$ [12, 13].

Fig. 1 shows an example of performed experiments in NSTX, with an $n = 1$ rotating magnetic perturbation with $f_a = +30Hz$ using midplane coils outside the chamber walls. The RFA signals are measured by B_R sensor arrays located slightly off the midplane. The plasmas are quiescent without any significant indication of tearing activity, which could produce additional torques and introduce nonideal layer responses.

The RFA measurements for Φ_w/Φ_w^x through these experiments are shown in Fig. 2 for (a) the amplitude and (b) the toroidal phase shift. Each point indicates the average over $100ms$, with the standard deviations represented by lines. The resulting RFA amplitudes almost linearly increase along with β_N, and are larger with the co-rotating magnetic field, as consistent with other RFA observations [11–14].

In the range of the standard deviations, various linear fits for the amplitude as a function of β_N, $(\Phi_w/\Phi_w^x)(\beta_N)$ can be found for each frequency $f_a = \pm 30Hz$. Using the information for the amplitudes, the best fitting parameters for $s(\beta_N)$, $\alpha(\beta_N)$, $c(\beta_N)$ and $\gamma_w(\beta_N)$ can be investigated by the least square method, that is, by minimizing the errors in Equation (16). It is found that the procedure becomes more robust when one of $c(\beta_N)$ and $\gamma_w(\beta_N)$ is given by a constant independent of β_N, and so when using three parameters in the minimization. Since the coupling coefficient c is easier to assume an approximate value, $c(\beta_N) \sim c$ is used in our investigation. Note that it is also possible to take both $c(\beta_N) \sim c$ and $\gamma_w(\beta_N) \sim \gamma_w$, since they are dependent only on the shape of the dominant mode Φ_w, which is not expected to have large variations in the investigated range of β_N.

Another consideration is that the measured RFA in vacuum is not exactly Φ_w^x, but is $\Phi_w^x/(1 - in\omega_a/\gamma_{w0})$. As discussed later, the results indicate $|\omega_a/\gamma_w| < 0.3$, but also $\gamma_{w0} \equiv \gamma_w(\beta_N = 0)$ may be largely different from γ_w. Therefore, here the possibility $|1 - in\omega_a/\gamma_{w0}| > 1$ is also considered.

The discussed uncertainties can result in nonphysical or inconsistent parameters, so it is essential to discriminate relevant cases. So, three additional constraints are introduced in the fitting procedure, based on the previous observations for the peak of RFA in NSTX [12, 13], and also based on the range in the measured RFA phases in Fig. 2 (b). The absolute values of RFA phases can not be directly used due to the unknown $\phi = 0$ location, as previously mentioned, but the range of the toroidal phase shift is independent of the $\phi = 0$ location.

In summary, the derivation of the four parameters $s(\beta_N)$, $\alpha(\beta_N)$, $c(\beta_N)$ and $\gamma_w(\beta_N)$ from RFA measurements is done with

1. The various linear fits for the RFA amplitudes at each frequency $f_a = \pm 30Hz$ are used within the standard deviations.

2. The $c(\beta_N) \sim c > 0.1$ is assumed and scanned.

3. The measured Φ_w^x is scanned within $1.0 \leq |1 - in\omega_a/\gamma_{w0}| \leq 1.5$ in order to allow uncertainties up to 50%.

4. With the various combinations of 1 to 3, the three parameters $s(\beta_N)$, $\alpha(\beta_N)$, and $\gamma_w(\beta_N)$ are found by least square method using Equation (16).

5. The determined four parameters are used to reconstruct the RFA amplitudes at the highest $\beta_N \approx 4.7$ as a function of f_a, and are retained when the peak is found within $f_a = +30 \sim +60Hz$.

6. The determined four parameters are used to reconstruct the RFA phases at the two frequencies $f_a = \pm 30Hz$, and are retained when the range of variations are consistent with the measured RFA phases within the standard deviations, which are $10.7^\circ < \Delta\phi(+30Hz) < 27.5^\circ$ and $16^\circ < \Delta\phi(-30Hz) < 32^\circ$.

Fig. 3 shows the reconstructed RFA using the average values of the retained four parameters. One can see that the constraints based on observations, as described in 5 and 6 of the fitting procedure, are satisfied with the reconstructions.

The coupling coefficient is found as $c = 0.18 \pm 0.05$, and the effective wall time $\tau_w = 1/\gamma_w$ as a function of β_N is shown in Fig. 4. As previously mentioned, the resulting τ_w corresponds to $|\omega_a/\gamma_w| < 0.3$, but also indicates that the $\tau_{w0} = 1/\gamma_{w0}$ may become larger. It is not relevant to extend the results based on our linear analysis to a very low β_N or to vacuum, so it should be clarified by direct vacuum measurements in the future. The derived γ_w is faster than the typical RWM growth rate $\gamma_{RMW} \sim (2.5 \sim 5.0ms)^{-1}$, but slower than the fast RWM growth rate $\gamma_{RMW} \sim (0.6ms)^{-1}$ in NSTX [12, 13, 25].

The energy and torque parameters derived from RFA measurements, (s_E, α_E), are shown in Fig. 5. The standard deviations become larger in lower β_N, indicating the sensitivity of the results depending on the fitting procedure. The (s_E, α_E) becomes more robust in

high β_N values and are consistent with the increase of the amplitudes of RFA. The plasma response at the boundary is $\Phi = -\Phi^x/(s + i\alpha)$, and so generally s and α must be decreased to increase RFA although the precise results at the magnetic sensors are more complicated by the wall-plasma coupling and wall constant represented by c and γ_w.

There are important implications in Fig. 5. If the currents associated with the torque are ignorable, $|s_E|$ would cross zero around the marginally stable point. However, the $|s_E|$ is far from zero even above the marginally stable point that can be found in $4.0 < \beta_N < 4.5$, and this implies that the perturbations are no longer able to optimally tap energy from the plasma. This is because $|\alpha_E|$ in Fig. 5 (b) is not so small and becomes comparable to $|\alpha_E| \sim |s_E| \sim 0.1$ above the marginally stable point. That is, the currents associated with the torque can change the perturbations, which is expected from the general relation of the plasma response as explained with Eq. (7) in Sec. II. When the currents associated with the torque become important, the energy $|s_E|$ would increase and $|\alpha_E|$ decrease compared to the expectations by scalar pressure equilibria as will be discussed in Sec. V. Also, the results may indicate that $|s_E|$ and $|\alpha_E|$ are adjusted similarly to each other, that is, to the phase shift 45° between Φ and Φ^x, but no theoretical explanation exists for this speculation yet.

V. COMPARISON WITH THEORETICAL CALCULATION

The theoretical evaluation for s_T can be directly obtained by IPEC calculations since IPEC is based on DCON stability code [26], which gives δW. However, even the fundamental values in scalar pressure equilibria, δW, can be sensitive to the reconstructions of experimental equilibria, and would have greater impacts on the calculations of α_T since the torque is quadratically proportional to the variation in the field strength. The calculations in this paper used the most advanced method for the reconstruction of NSTX equilibria, including Motional Stark Effect (MSE) measurements of q profiles and the averaged rotational effects, but it is still pending how to reconstruct experimental equilibria to be consistent with all the measured kinetic profiles. In order to investigate the level of sensitivity in the results, the calculations are performed based on a number of reconstructions in every $20ms$, and shown by mean values over $100ms$ with the standard deviations, Fig. 6.

A self-consistent calculation for the toroidal torque α_T is not presently available in IPEC,

since the currents associated with the torque and the shielding by the torque are not retained in a scalar pressure IPEC analysis. Note the scalar pressure equilibria do not have a torque since a mathematical identity implies the torque between any two constant pressure surfaces vanishes, $\int(\vec{x}\times\vec{\nabla}p)d^3x=0$, which is equivalent to $\alpha_T=0$. However, one can use the scalar pressure IPEC for the field if $|\alpha_T| << |s_T|$, that is, if the currents associated with the torque can be ignorable.

The toroidal torque can be evaluated theoretically if one couples the IPEC field to a relevant model for transport. Here the theory of nonambipolar transport [16–19] is used to evaluate the radial currents and so the toroidal torque. In tokamaks, this is so called Neoclassical Toroidal Viscoscity (NTV) torque [17, 18], which has been found as the dominant drive for the torque [27] in the presence of nonaxisymmetric perturbations. Compared with the previous theory, here the actual *Lagrangian* variation in the field strength $\delta B=\delta B_E+\vec{\xi}\cdot\vec{\nabla}B_0$ [28], where $\vec{\xi}$ is the plasma displacement, is used instead of the perturbed field δB_E at a fixed spatial point. The Lagrangian variation in the field strength obtained by IPEC is coupled with recently derived general NTV formula [19], which includes the additional effects by the resonance between bouncing orbits and precessions, to estimate the transport and the torque. Although the precise assessment of NTV transport is still an active area of research, any formula gives $\tau_\varphi\propto\delta B^2$. The variations of the torque, and so α_T, are largely determined by the variations of δB^2 in the studied range of β_N, where the variations of kinetic parameters related to the NTV theory are relatively small.

The calculated (s_T,α_T) is shown in Fig. 6, and is compared with the empirically evaluated (s_E,α_E). As can be seen, Fig. 6 shows the shielding by the torque is ignorable and IPEC method is approximately valid when both $|\alpha_E|<|s_E|$ and $|\alpha_T|<|s_T|$, as can be found in low β_N values, within acceptable deviations between each other. The deviations between empirical and theoretical values at the lowest β_N are not trivial and the reason is unclear, but the large standard deviation in empirical values indicates that the results may be unreliable due to the sensitivity in the fitting procedure. The obvious inconsistency occurs when $|\alpha|\geq|s|$ beyond the marginally stable β_N. The differences between s_E and s_T in Fig. 6 (a) seems small, but the relative ratio is very large since $s_T\approx 0$. The deviations of α_T from α_E is apparent from in Fig. 6 (b).

The deviations between (s_E,α_E) and (s_T,α_T) are due to the currents associated with the torque that are missing in IPEC. The results indicate that the stabilizing effect in s_E and

the shielding effect in α_E can occur by the torque, as expected in Sec. II. If the currents associated with the torque are not included, the calculations of perturbed equilibria such as the present IPEC can become largely inconsistent when $|\alpha| \geq |s|$, or equivalently when plasma is close to the $n = 1$ marginal limit of ideal stability. The higher n has the higher β_N required to be marginal stable, so $|\alpha| << |s|$ can be expected and thus the scalar pressure perturbed equilibria may be good approximations for most of applications with $n \geq 3$ perturbations, as should be studied in the future.

VI. CONCLUDING REMARKS

The exact relation of plasma response is described and the simplified relation based on a single dominant mode with (s, α) is used to compare RFA measurements in NSTX with IPEC calculations coupled with the theory of nonambipolar transport. Although the nontrivial uncertainties are involved in both experimental and theoretical derivations of (s, α), it is found that the currents associated with the torque can be ignored and the calculations of perturbed scalar pressure equilibria are approximately valid when $|\alpha| < |s|$, but can be largely inconsistent when $|\alpha| \geq |s|$. It implies that the shielding currents associated with the torque should be considered in perturbed equilibria when $|\alpha| \geq |s|$, and when plasma is beyond the marginally stable limit. Therefore, the tensor pressure equilibria $\vec{\nabla} \cdot \overleftrightarrow{p} = \vec{j} \times \vec{B}$ must be solved to give fully self-consistent descriptions of plasma response in high β_N plasmas, as will be important for many applications such as RWM feedback control.

Acknowledgments

This work was supported by DOE contract DE-AC02-76CH03073 (PPPL), and DE-FG02-03ERS496 (CU).

[1] K. Ikeda, Nucl. Fusion **47**, S1 (2007).

[2] T. C. Hender, R. Fitzpatrick, A. W. Morris, P. G. Carolan, R. D. Durst, T. Eddlington, J. Ferreira, S. J. Fielding, P. S. Haynes, J. Hugill, I. J. Jenkins, R. J. La Haye, B. J. Parham, D. C. Robinson, T. N. Todd, M. Valovic, and G. Vayakis, Nucl. Fusion **32**, 2091 (1992).

[3] R. J. La Haye, R. Fitzpatrick, T. C. Hender, A. W. Morris, J. T. Scoville, and T. N. Todd, Phys. Fluids B **4**, 2098 (1992).

[4] R. J. Buttery, M. D. Benedetti, D. Gates, Y. Gribov, T. Hender, R.J. La Haye, P. Leahy, J. Leuer, A. Morris, A. Santagiustina, J. Scoville, B. J. D. Tubbing, the JET Team, the COMPASS-D Research Team, and the DIII-D Team, Nucl. Fusion **39**, 1827 (1999).

[5] M. Okabayashi, J. Bialek, M. S. Chance, M. S. Chu, E. D. Fredrickson, A. M. Garofalo, R. Hatcher, T. H. Jensen, L. C. Johnson, R. J. LaHaye, G. A. Navratil, H. Reimerdes, J. T. Scoville, E. J. Strait, A. D. Turnbull, M. L. Walker, and the DIII-D Team, Plasma Phys. Controlled Fusion **44**, B339 (2002).

[6] T. E. Evans, R. A. Moyer, P. R. Thomas, J. G. Watkins, T. H. Osborne, J. A. Boedo, E. J. Doyle, M. E. Fenstermacher, K. H. Finken, R. J. Groebner, M. Groth, J. H. Harris, R. J. La Haye, C. J. Lasnier, S. Masuzaki, N. Ohyabu, D. G. Pretty, T. L. Rhodes, H. Reimerdes, D. L. Rudakov, M. J. Schaffer, G. Wang, and L. Zeng, Phys. Rev. Lett. **92**, 235003 (2004).

[7] J.-K. Park, A. H. Boozer, and A. H. Glasser, Phys. Plasmas **14**, 052110 (2007).

[8] J.-K. Park, M. J. Schaffer, J. E. Menard, and A. H. Boozer, Phys. Rev. Lett. **99**, 195003 (2007).

[9] J.-K. Park, A. H. Boozer, J. E. Menard, A. M. Garofalo, M. J. Schaffer, R. J. Hawryluk, S. M. Kaye, S. P. Gerhardt, S. A. Sabbagh, and the NSTX team, Phys. Plasmas **16**, 056115 (2009).

[10] A. H. Boozer, Phys. Rev. Lett. **86**, 5059 (2001).

[11] H. Reimerdes, T. C. Hender, S. A. Sabbagh, J. M. Bialek, M. S. Chu, A. M. Garofalo, M. P. Gryaznevich, D. F. Howell, G. L. Jackson, R. J. La Haye, Y. Q. Liu, J. E. Menard, G. A. Navratil, M. Okabayashi, S. D. Pinches, A. C. Sontag, E. J. Strait, W. Zhu, M. Bigi, M. de Baar, P. de Vries, D. A. Gates, P. Gohil, R. J. Groebner, D. Mueller, R. Raman, J. T. Scoville, W. M. Solomon, the DIII-D Team, JET-EFDA Contributors, and the NSTX Team, Phys. Plasmas **13**, 056107 (2006).

[12] A. C. Sontag, S. A. Sabbagh, W. Zhu, J. M. Bialek, J. E. Menard, D. A. Gates, A. H. Glasser, R. E. Bell, B. P. LeBlanc, M. G. Bell, A. Bondeson, J. D. Callen, M. S. Chu, C. C. Hegna, S. M. Kaye, L. L. Lao, Y. Liu, R. Maingi, D. Mueller, K. C. Shaing, D. Stutman, and K. Tritz, Phys. Plasmas **12**, 056112 (2005).

[13] A. Sontag, S. Sabbagh, W. Zhu, J. Menard, R. Bell, J. Bialek, M. Bell, D. Gates, A. Glasser, B. LeBlanc, K. Shaing, D. Stutman, and K. Tritz, Nucl. Fusion **47**, 1005 (2007).

[14] A. M. Garofalo, G. L. Jackson, R. J. La Haye, M.Okabayashi, H. Reimerdes, E. J. Strait, J. R. Ferron, R. J. Groebner, Y. In, M. J. Lanctot, G. Matsunaga, G. A. Navratil, W. M. Solomon, H. Takahashi, M. Takechi, A. D. Turnbull, and the DIII-D Team, Nucl. Fusion **47**, 1121 (2007).

[15] M. Ono, S. Kaye, Y.-K. Peng, G. Barnes, W. Blanchard, M. Carter, J. Chrzanowski, L. Dudek, R. Ewig, D. Gates, R. Hatcher, T. Jarboe, S. Jardin, D. Johnson, R. Kaita, M. Kalish, C. Kessel, H. Kugel, R. Maingi, R. Majeski, J. Manickam, B. McCormack, J. E. Menard, D. Mueller, B. Nelson, B. Nelson, C. Neumeyer, G. Oliaro, F. Paoletti, R. Parsells, E. Perry, N. Pomphrey, S. Ramakrishnan, R. Raman, G. Rewoldt, J. Robinson, A. Roquemore, P. Ryan, S. A. Sabbagh, D. Swain, E. Synakowski, M. Viola, M. Williams, J. Wilson, and the NSTX Team, Nucl. Fusion **40**, 557 (2000).

[16] R. Linsker and A. H. Boozer, Phys. Fluids **25**, 143 (1982).

[17] K. C. Shaing, Phys. Plasmas **10**, 1443 (2003).

[18] K. C. Shaing, P. Cahyna, M. Becoulet, J.-K. Park, S. A. Sabbagh, and M. S. Chu, Phys. Plasmas **15**, 082506 (2008).

[19] J.-K. Park, A. H. Boozer, and J. E. Menard, Phys. Rev. Lett. **102**, 065002 (2009).

[20] A. H. Boozer, Phys. Plasmas **10**, 1458 (2003).

[21] I. H. Hutchinson, Plasma Phys. Controlled Fusion **43**, 145 (2001).

[22] A. H. Boozer, Phys. Plasmas **16**, 052505 (2009).

[23] J. Bialek, A. H. Boozer, M. E. Mauel, and G. A. Navratil, Phys. Plasmas **8**, 2170 (2001).

[24] J.-K. Park, A. H. Boozer, J. E. Menard, and M. J. Schaffer, Nucl. Fusion **48**, 045006 (2008).

[25] S. A. Sabbagh, R. E. Bell, J. E. Menard, D. A. Gates, A. C. Sontag, J. M. Bialek, B. P. LeBlanc, F. M. Levinton, K. Tritz, and H. Yuh, Phys. Rev. Lett. **97**, 045004 (2006).

[26] A. H. Glasser and M. S. Chance, Bull. Am. Phys. Soc. **42**, 1848 (1997).

[27] W. Zhu, S. A. Sabbagh, R. E. Bell, J. M. Bialek, B. P. LeBlanc, S. M. Kaye, F. M. Levinton, J. E. Menard, K. C. Shaing, A. C. Sontag, and H. Yuh, Phys. Rev. Lett. **96**, 225002 (2006).

[28] A. H. Boozer, Phys. Plasmas **13**, 044501 (2006).

List of Figures

Figures

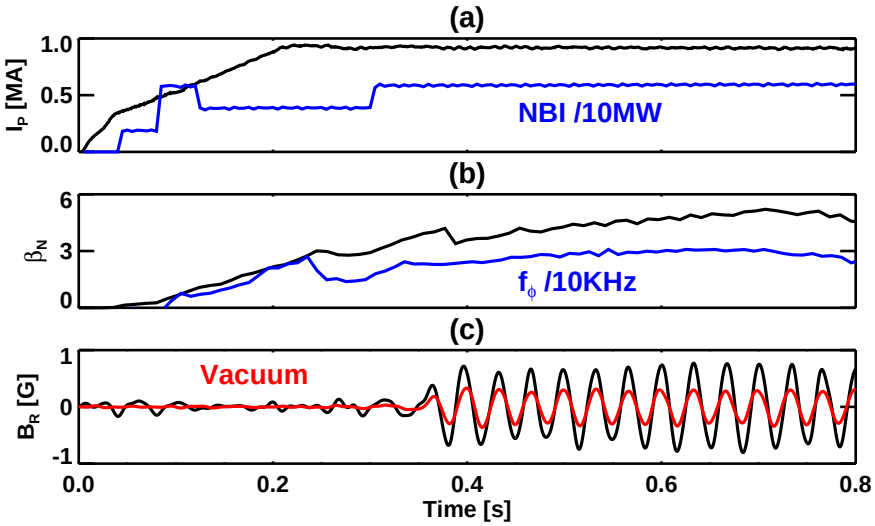

FIG. 1: (COLOR) The experiments for RFA, Φ_w/Φ_w^x, measurements in a rotating NSTX plasma. (a) shows the plasma current I_p (black) and the Neutral Beam Injection power (blue). (b) shows the normalized plasma pressure β_N (black) and the plasma rotation frequency f_ϕ in the core region (blue), and (c) shows the $n = 1$ filtered signal in B_R sensor arrays for Φ_w (black, #124801) and Φ_w^x (red, #125235).

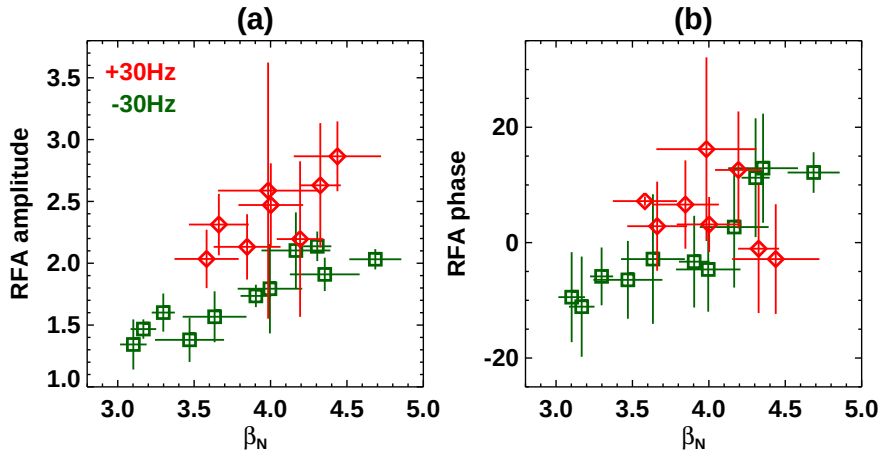

FIG. 2: (COLOR) The measured Φ_w/Φ_w^x by applied $n = 1$ rotating fields at two frequencies, $f_a = +30Hz$ (red, $\diamond$) and $-30Hz$ (green, $\square$) as a function of β_N. (a) shows the amplitudes of RFA and (b) shows the toroidal phases of RFA in terms of normal angle (°). The lines across each data point indicate the standard deviations when averaged over $100ms$.

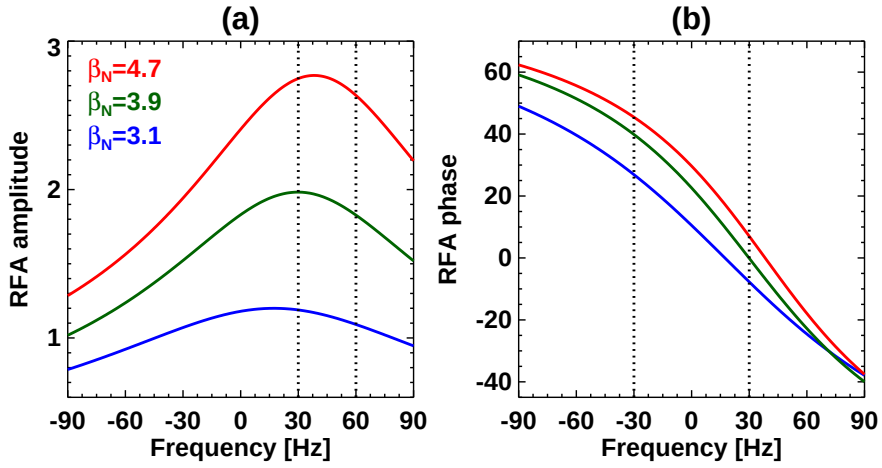

FIG. 3: (COLOR) The reconstructed RFA as a function of the applied frequency f_a for (a) the amplitude and (b) the toroidal phase (°), using the mean values of $s(\beta_N)$, $\alpha(\beta_N)$, c and $\gamma_w(\beta_N)$. Three reconstructions for $\beta_N \approx 3.1$ (blue), $\beta_N \approx 3.9$ (green), and $\beta_N \approx 4.7$ are shown. The peak of the RFA at the highest $\beta_N \approx 4.7$ in (a) can be found around $38Hz$, which is within $30Hz \sim 60Hz$ (indicated by dotted lines), as consistent with other observations. Also, the reconstructed phase is consistent with the range of the measured phases at two frequencies $f_a = \pm 30Hz$ (indicated by dotted lines), as described in 6 of the fitting procedure.

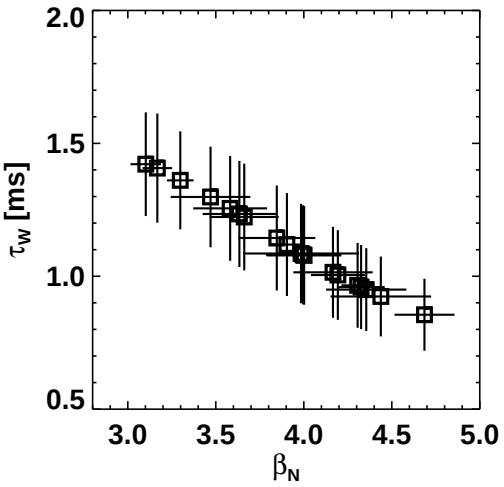

FIG. 4: The empirical wall constant $\tau_W(\beta_N)$ derived from RFA measurements. The results indicate that the wall constant may be largest in vacuum, but decrease along with β_N due to the change in the shape of the field distribution.

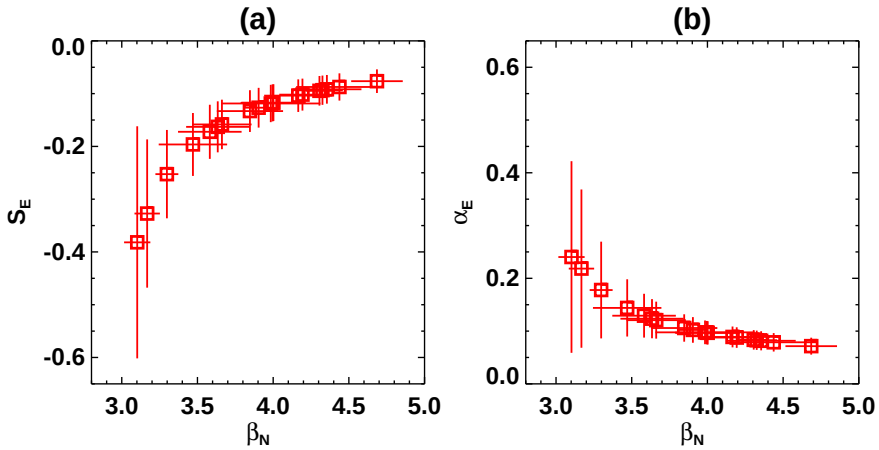

FIG. 5: (COLOR) The empirical (a) $s_E(\beta_N)$ and (b) $\alpha_E(\beta_N)$ derived from RFA measurements. The large standard deviations in low β_N values indicate the sensitivity of the results to the fitting procedure, but the results become robust in high β_N values. Note that the empirical energy s_E remains negative and never crosses zero even beyond the marginally stable point, and that the empirical torque α_E decreases along with β_N.

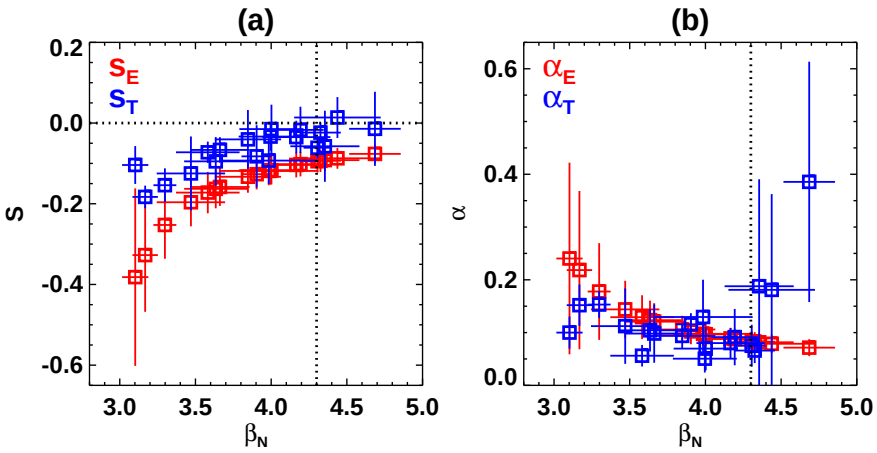

FIG. 6: (COLOR) Comparison between (a) s_E (red) and s_T (blue), and (b) α_E (red) and α_E (blue). Note the reasonable agreement between the measurement and the theory when $|\alpha| < |s|$, and the large inconsistency when $|\alpha| \geq |s|$ for both s and α. The point of discrepancy is indicated by the lines at $\beta_N \sim 4.3$, which is within the marginally stable point, $4.0 < \beta_N < 4.5$. One can see that $s_T \to 0$, but s_E remains finite, so the relative ratio becomes very large. The deviations of α_T from α_E are more apparent. This discrepancy is expected since the currents associated with the torque are not included in scalar pressure equilibria. It can be seen the additional (a) stabilizing effect in s_E and (b) shielding effect in α_E by the torque.

The Princeton Plasma Physics Laboratory is operated
by Princeton University under contract
with the U.S. Department of Energy.

Information Services
Princeton Plasma Physics Laboratory
P.O. Box 451
Princeton, NJ 08543

Phone: 609-243-2750
Fax: 609-243-2751
e-mail: pppl_info@pppl.gov
Internet Address: http://www.pppl.gov